Longitudinally Dependent Ozone Increase in the Antarctic Polar Vortex Revealed by Balloon and Satellite Observations

K. SATO

Department of Earth and Planetary Science, The University of Tokyo, Tokyo, Japan

Y. TOMIKAWA, G. HASHIDA, AND T. YAMANOUCHI

National Institute of Polar Research, Tokyo, Japan

H. NAKAJIMA AND T. SUGITA

National Institute for Environmental Studies, Ibaraki, Japan

(Manuscript received 29 July 2008, in final form 15 November 2008)

ABSTRACT

The horizontal structure of processes causing increases in ozone in the Antarctic polar vortex was examined using data measured in 2003 from an ozonesonde observation campaign at Syowa Station (39.6°E, 69.0°S) and from the Improved Limb Atmospheric Spectrometer II (ILAS-II) onboard the *Advanced Earth Observing Satellite II*. The ILAS-II data are daily and distributed uniformly at 14 points in the zonal direction, mostly at polar latitudes. The Antarctic ozone hole that developed in 2003 was one of the largest recorded. The period of focus in this study is 26 September through 24 October, when a strong polar vortex was situated in the stratosphere. An ozone mixing ratio contour (1.0 ppmv) moved downward near a height of 20 km during the period of focus. This increase in ozone is likely to result from downward transport of ozone-rich air originating from lower latitudes by Brewer–Dobson circulation. First, the descent rate of the mixing ratio contour was estimated by taking the geometric height as the vertical coordinate for the deep vortex interior around 20 km. A significant longitudinal dependence was observed. An analysis using ECMWF operational data shows that this dependence can be approximately explained by longitudinally dependent vertical movements of the isentropes caused by a zonal wavenumber-1 quasi-stationary planetary wave with amplitude and phases varying on a seasonal time scale. Next, the descent rate was calculated around 500 K (around 20 km) by taking the potential temperature (isentrope) as the vertical coordinate. The longitudinal dependence was still present using this coordinate, meaning that the ozone mixing ratio and its increase are not constant on the isentropic layer even in the interior of the polar vortex. A backward trajectory analysis showed that air parcels with large ozone mixing ratios were mostly transported from the polar vortex boundary region. This result suggests that lateral transport/mixing is important even before the breakup of the polar vortex. Results from a tracer–tracer correlation analysis of O_3 and long-lived constituent N_2O were also consistent with this inference. The contribution of lateral mixing to the increase in ozone was estimated at about 17% $\pm$ 4% that of the Brewer–Dobson circulation around 20 km, using the calculated descent rates. The results of this study also imply that Lagrangian downward motions in the vortex interior are not correctly estimated without accounting for lateral mixing, even if the polar vortex is dynamically stable.

1. Introduction

Following the first reports of significant depletion of ozone in the Antarctic spring made independently by Chubachi (1984) and Farman et al. (1985), much scientific research by aircraft missions, balloon and satellite observations, and laboratory studies has been devoted to exploring the formation mechanism of the Antarctic ozone hole in terms of chemical, dynamical, and radiative processes [see a review paper by Solomon (1999) for details]. In the Antarctic winter and early spring, the stratospheric temperature is sufficiently low to form so-called polar stratospheric clouds (PSCs). In such a cold

Corresponding author address: Kaoru Sato, Department of Earth and Planetary Science, The University of Tokyo, Tokyo 113–0033, Japan.
E-mail: kaoru@eps.s.u-tokyo.ac.jp

DOI: 10.1175/2008JAS2904.1

environment, the conversion from ClO_x reservoirs such as HCl and $ClNO_3$ to Cl_2 is effective. The molecular chlorine Cl_2 rapidly photolyzes to form ClO_x as the sun rises over Antarctica. It has been shown that the combination of catalytic cycles including ClO dimer and BrO + ClO accounts for most of the ozone destruction in the Antarctic spring (Molina and Molina 1987; McElroy et al. 1986; Tung et al. 1986). The reaction speeds of these cycles are still controversial (Pope et al. 2007; von Hobe et al. 2007). Another important process for the ozone hole formation is the removal of HNO_3 from the stratosphere in association with sedimentation of PSCs. This denitrification process prohibits ClO_x from reforming its reservoir in spring and allows further ozone destruction (e.g., Jacob 1999). As a result, the area of the Antarctic ozone hole is usually maximized from late September through early October.

The dissipation of the Antarctic ozone hole (i.e., ozone increase after the maximum stage of the ozone hole) is considered to be mainly controlled by dynamics (e.g., Shepherd 2007). In late spring, the polar vortex, which isolates ozone-poor air inside, becomes unstable and breaks up. Then the ozone-rich air from the lower latitudes intrudes into, and is mixed with, the ozone-poor air in the polar region, mostly horizontally by adiabatic processes with time scales of O(1–10) days. The Antarctic ozone hole disappears in either November or December depending on the year.

Ozone-rich air originating from lower latitudes is also gradually transported downward to the polar lower stratosphere in association with diabatic circulation (Brewer–Dobson circulation) with a time scale of O(100–1000) days. The downward flow of the Brewer–Dobson circulation in the polar region was examined by previous studies using long-lived trace species such as N_2O, CH_4, and HF (Schoeberl et al. 1995; Kawamoto and Shiotani 2000; Kawamoto et al. 2004, and references therein). The Brewer–Dobson circulation is driven by the wave-induced force through the ''downward control'' mechanism and hence is modified by the characteristics of the wave force such as its strength and time scales (e.g., Holton et al. 1995). The downward flow in the polar region, therefore, depends on altitude and season (Rosenfield et al. 1994; Abrams et al. 1996). Manney et al. (1995) showed that the downward transport of ozone-rich air in association with the Brewer–Dobson circulation largely masked the chemical ozone depletion above the 520-K level (corresponding to an altitude of about 21 km) in late August and early September 1992. The downward transport is also important in late September and October, the period of focus in the present study, because it replenishes ozone in the Antarctic ozone hole region.

In this study, downward transport is examined in two ways: the first uses the descent rate of a particular mixing ratio contour of ozone and long-lived species of N_2O and CH_4 relative to the geometric height, and the second is relative to the potential temperature. The first method provides a view of circulation in geometric space and allows comparison with the residual circulation using the transformed Eulerian mean equation system (e.g., Andrews et al. 1987). The second highlights the diabatic component of the downward motion, although the direction can be opposite to the vertical motion in geometric space, particularly in spring when the isentropic surfaces themselves move downward geometrically because of radiative heating.

Analyses in previous studies have been made by assuming implicitly that the mixing ratios of minor constituents are almost constant in the polar vortex. However, this assumption may not be the case. The purpose of this study is to examine the horizontal structure of ozone increase processes after the area of the Antarctic ozone hole is maximized, based on balloon and satellite observations. Data from an intensive ozonesonde observation campaign performed at Syowa Station (69.0°S, 39.6°E) from mid-June 2003 to early January 2004 were used, as were data in the high-latitude stratosphere recorded by the Improved Limb Atmospheric Spectrometer II (ILAS-II) onboard the *Advanced Earth Observing Satellite-II* (*ADEOS-II*) from early April through late October 2003 (Nakajima et al. 2005, 2006; Sugita et al. 2006). These two observational datasets are complementary: the ozonesonde observation data have very fine vertical resolution (about 50 m), whereas the satellite data include long-lived trace species such as N_2O and CH_4 as well as ozone with relatively fine vertical resolution (about 1 km) distributed over a wide horizontal area. The present study focuses on the time period from 26 September through 24 October 2003, when a strong polar vortex was present in the stratosphere, because of the limited period of satellite observation data. The end of this time period was 1 month prior to polar vortex breakup. During this period, a clear downward movement of a particular mixing ratio contour was observed near a height of 20 km for ozone and the long-lived species N_2O and CH_4, suggesting downward transport. Following Nash et al. (1996), observation data were categorized into three groups: those from the deep vortex interior, those in the vortex boundary region, and those outside the polar vortex. Only data in the deep vortex interior were used for the descent rate analysis. Hereafter, the observed descent rates of these minor constituent contours are referred to as O_3 descent rates, N_2O descent rates, and CH_4 descent rates, respectively, to distinguish from the ''true''

descent rate corresponding to downward motion of the Brewer–Dobson circulation. The maximum area of the Antarctic ozone hole in 2003 was one of the largest recorded. Thus, the seasonal-scale ozone layer recovery processes analyzed in the present study are considered typical for the Antarctic.

The life cycle of the Antarctic ozone hole in 2003 and details of the ozonesonde observation at Syowa Station and ILAS-II observation are described in section 2. Seasonal variation of the stratospheric polar vortex in the Southern Hemisphere in 2003 is documented in section 3. In section 4, the O_3, N_2O, and CH_4 descent rates are shown as a function of longitude by taking geometric height as the vertical coordinate, and the observed longitudinal dependence is interpreted in terms of slowly varying quasi-stationary planetary waves. In section 5, the descent rates are calculated by taking the potential temperature as the vertical coordinate, and the remaining longitudinal dependence is examined in terms of the lateral mixing. A summary and concluding remarks are presented in section 6.

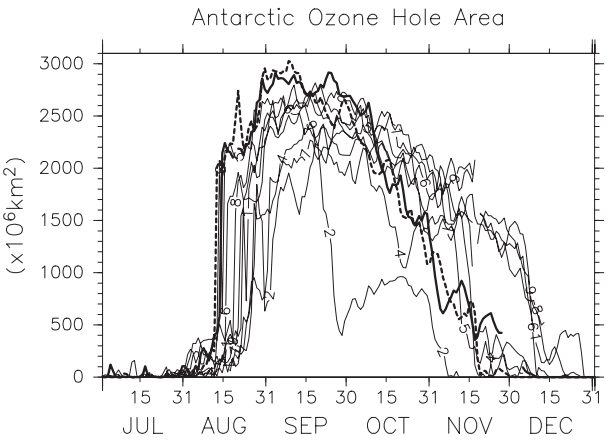

FIG. 1. Time variations in the size of the Antarctic ozone hole from 1996 to 2005. Numerals on each curve indicate the last digit of each year (e.g., 6 and 5 indicate the profiles for 1996 and 2005, respectively). The thick solid curve and thick dashed curve show profiles in 2003 and 2000, respectively. Data were provided by the Japan Meteorological Agency.

2. Characteristics of the Antarctic ozone hole in 2003 and description of balloon and satellite observations

Time series of the area of the ozone hole (defined as the area with total column ozone values smaller than 220 Dobson units) in July through December for 1996–2005 are shown in Fig. 1. In 2003, the ozone hole developed rapidly in the second half of August, reached a maximum in late September, shrank gradually in October and November, and disappeared in early December (a thick solid curve). Such temporal variation is quite similar to that of the largest ozone hole observed in 2000 (a thick dashed curve).

An intensive observation campaign was performed at Syowa Station over about 7 months from mid-June 2003 through early January 2004, which covers the whole period of ozone hole formation and dissipation. The first half of the observations until mid-October at Syowa Station were made for the first ozonesonde network campaign in the Antarctic to examine ozone hole formation processes. This campaign was a part of the European project Quantitative Understanding of Ozone Losses by Bipolar Investigations (QUOBI; see, e.g., Rex et al. 2004) using the Match technique (von der Gathen et al. 1995). The network was composed of nine Antarctic stations: Neumayer, Rothera, Dumont d'Urville, Marambio, Belgrano, McMurdo, South Pole, Davis, and Syowa. Details of the Antarctic Match campaign will be reported elsewhere. During this period, 46 observations were successfully made using electrochemical concentration cell (ECC) ozonesondes (26 EnSci and 20 Science Pump ozonesondes connected with Vaisala RS-80GE radiosondes by Vaisala RSA-1 interfaces) at Syowa Station. The ozonesondes were launched a few times a week.

In the subsequent period until mid-December 2003, the intensive ozonesonde observation at Syowa Station continued in order to examine ozone hole dissipation processes. Forty Science Pump ECC ozonesondes were successfully launched by rubber balloons. The observation frequency was higher than in the ozone hole formation period because the stratospheric conditions vary on shorter time scales of days in association with the polar vortex breakup.

The success of an ozonesonde launch strongly depends on the weather conditions, which are not always favorable in the Antarctic. For regular observations, rubber balloons with a weight of 1500 g were used. A small hut for the balloon preparation at Syowa Station enabled successful launches in windy conditions up to 17 m s^{-1}. Moreover, to avoid the balloons bursting prematurely in the cold lower stratosphere from June to October, the balloons were dipped in kerosene and warmed prior to launch. The mean top altitude of observations was about 27 km. When the temperature increased in November and December, kerosene was not used. The balloons reached higher altitudes in these months (about 32 km on average). The percentage of successful launches during the whole observation campaign was about 90%.

In addition to the rubber balloon observations, seven high-altitude balloon observations were performed on

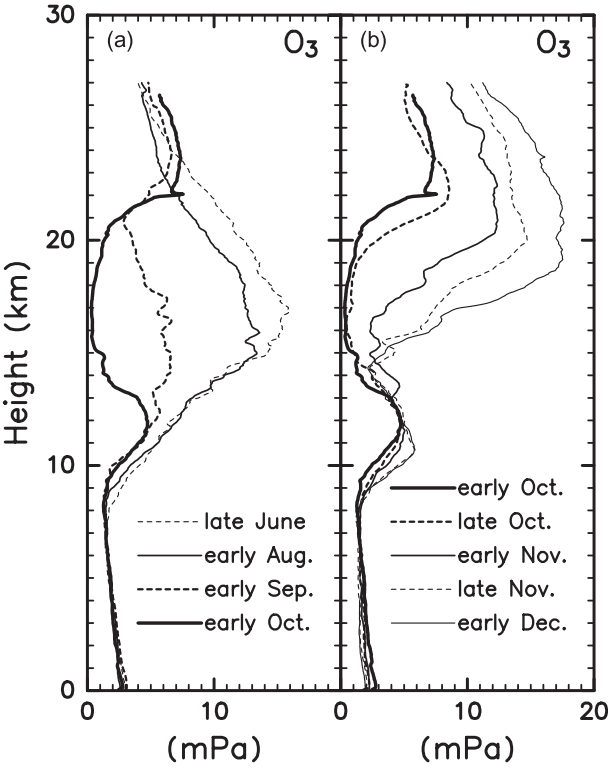

FIG. 2. Time variation of vertical profiles of ozone partial pressure averaged over 10 days at Syowa Station in the period of (a) formation and (b) dissipation of the Antarctic ozone hole in 2003.

7 and 18 November 2003; 5, 13, and 27 December 2003; and 6 and 9 January 2004. The high-altitude balloons used were made of very thin polyethylene films (5.6 μm) with a diameter of about 24 m and a length of about 33 m (a volume of about 5000 m^3) (Yamagami et al. 2004) and reached a height of about 40 km. Calm weather conditions with surface winds weaker than 3 m s^{-1} are required for a successful launch. An optical ozonesonde measuring vertical profiles of solar radiation at ultraviolet and visible wavelengths (Okano et al. 1996; Murata et al. 2004) retrieving the ozone profile in the middle and upper stratosphere was used together with an ECC ozonesonde for each high-altitude balloon observation. In this study, only the data from ECC ozonesonde observations are used for the analysis.

Figure 2 shows the time variation of vertical profiles of the ozone partial pressure before and after the area of the ozone hole was maximized in late September. Each profile is an average of observations over 10 days (e.g., ''late June'' means the time period of 21–30 June). In June, the ozone layer is present in the height region of 13–21 km. The ozone appears to be destroyed almost simultaneously throughout the ozone layer until early October. On the other hand, increases in ozone commenced earlier at higher altitudes. The ozone increase started in early September whereas the photochemical ozone destruction process continued below 21 km, which is consistent with findings of Manney et al. (1995). This point will be re-examined in the next section using the ozone mixing ratio (which is a conservative quantity in the absence of the sources and sinks of ozone and irreversible mixing). The ozone partial pressure remained small around the height of 14 km even after the ozone hole (i.e., a region with total column ozone values smaller than 220 Dobson units) disappeared in early November.

The horizontal structure of the processes causing increases in ozone was investigated using satellite data of ozone (Sugita et al. 2006) and the long-lived species N_2O and CH_4 (Ejiri et al. 2006) from ILAS-II onboard the ADEOS-II. ADEOS-II was launched on 14 December 2002, began observations on 2 April 2003, and finished operation on 24 October 2003 because of unexpected problems with the power supply system (Nakajima et al. 2006). The ADEOS-II satellite circumnavigated the earth about 14 times daily; thus, the ILAS-II observed occultations for 14 sunrises and 14 sunsets in the Northern and Southern Hemispheres, respectively. Measurements were made mostly at high latitudes, varying with season (54°–71°N and 64°–88°S). ILAS-II data processed by the version 1.4 retrieval algorithm were used for this study (http://www-ilas2.nies.go.jp). In the present study, we focused on the last 1-month period from 26 September to 24 October. Because the polar vortex breakup occurred from late November through early December depending on the altitude as shown in section 3, the processes causing ozone increase were examined when a strong polar vortex was situated in the stratosphere. Dynamical characteristics of the polar vortex and planetary waves are examined utilizing the 4 times daily global operational data provided by European Centre for Medium-Range Weather Forecasts (ECMWF).

3. Seasonal variation of the stratosphere in 2003

The life cycle of the ozone hole is largely affected by the seasonal variation of the stratospheric polar vortex. Figure 3 shows the mean speed of horizontal winds (hatches) along the potential vorticity contour (i.e., tangential winds) on the isentropic surface of 500 K as a function of time and equivalent latitude for March 2003 through January 2004. Here, the equivalent latitude is defined using the potential vorticity. The potential vorticity values are also shown by contours in Fig. 3. The isentropic surface of 500 K roughly corresponds to the altitude of 20 km where the ozone increase is clearly observed on a seasonal time scale (Fig. 2).

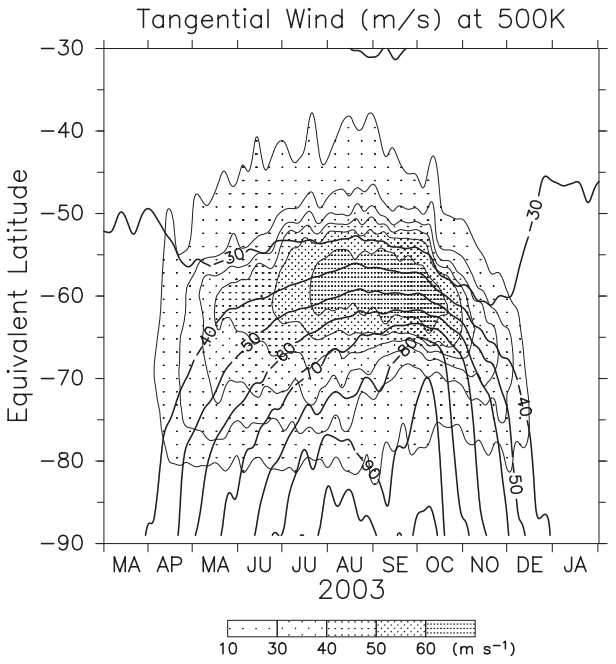

FIG. 3. A time and equivalent lat section of the potential vorticity (contours) and tangential wind speeds (hatches) along the potential vorticity contours at 500 K ($z \sim 20$ km). Contour interval is 10 PVU (1 PVU $\equiv 10^{-6}$ K kg^{-1} m^2 s^{-1}). A low-pass filter with a cutoff length of 10 days was applied.

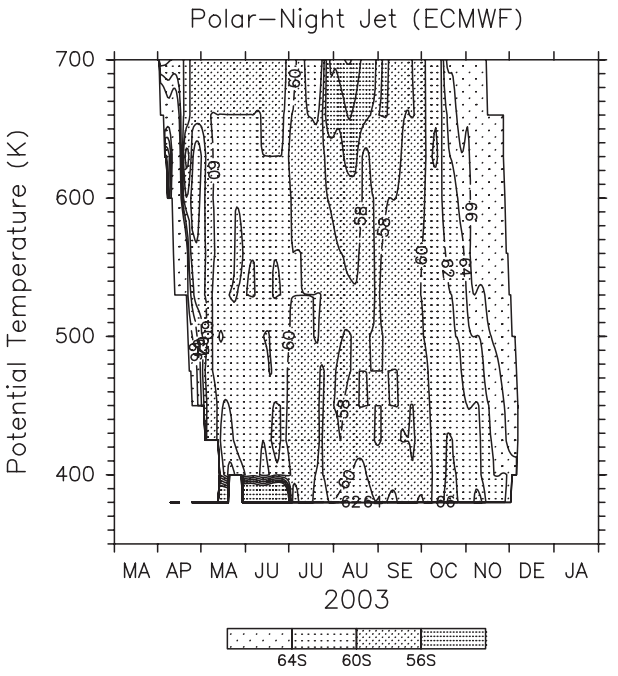

FIG. 4. A time and potential temperature section of the equivalent lat of the polar vortex edge as determined by the definition of Nash et al. (1996).

The polar night jet is observed around an equivalent latitude of 60°S in winter and spring. The tangential winds are greater than 50 m s^{-1} from the end of June through to the end of October. The polar night jet gradually weakens in November and disappears in early December. The jet axis propagates gradually poleward (i.e., the polar vortex is getting smaller) in October and November.

Figure 4 shows seasonal variation of the equivalent latitude of polar vortex edge, which is defined following Nash et al. (1996), as a function of potential temperature over the same time period as in Fig. 3. The regions when and where the polar vortex is present are hatched. The polar vortex forms in autumn and breaks up in spring at higher altitudes earlier than at lower altitudes. This feature of the polar vortex breakup is consistent with the earlier increase of ozone at higher altitudes in November and December observed by the ozonesondes at Syowa Station (Fig. 2).

However, the increase in ozone observed above 21 km starting in early September, as mentioned in section 2 (Fig. 2), is not attributed to the polar vortex breakup. The polar vortex is strong and dynamically stable in the period of focus from 26 September to 24 October 2003.

4. Longitudinal dependence of ozone increase in the geometric vertical coordinate

a. Descent rates in the geometric vertical coordinate

The increase in ozone observed before the polar vortex breakup is considered to mostly result from the diabatic transport of ozone-rich air from lower latitudes by the Brewer–Dobson circulation, whereas that observed after is mostly due to adiabatic intrusion of and mixing with lower-latitude air in association with the polar vortex breakup.

The mixing ratios of minor constituents are conserved when their sources, sinks, and irreversible mixing processes are absent. Thus, a time–height section of the ozone mixing ratio from ozonesonde observations at Syowa Station is shown in Fig. 5. Thick dashed curves show the isotherms of −80°C, roughly indicating possible PSC areas. The ozone mixing ratio decreases rapidly in August and September below about 20 km because of photochemical ozone destruction reactions. The ozone mixing ratio increases suddenly in November above about 15 km, likely because of the intrusion of ozone rich air from midlatitudes in association with a largely distorted polar vortex in its breaking stage.

An important feature seen before November is that the mixing ratio increases gradually after August in the height region of 20–23 km. In other words, the mixing ratio

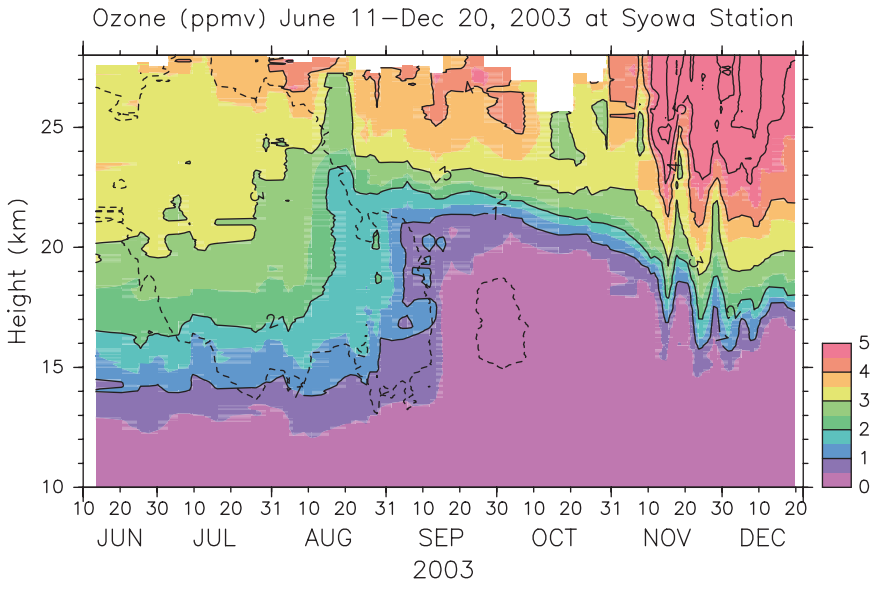

FIG. 5. A time–height section of ozone mixing ratio (colors) from ozonesonde observations at Syowa Station in 2003. Thick dashed curves show the −80°C isotherms, roughly indicating possible polar stratospheric cloud areas.

contour moves downward. This feature corresponds to the earlier ozone increase at higher altitudes as indicated in Fig. 2 and is probably due to the downward transport of ozone by the Brewer–Dobson circulation. The descent rate for the O_3 contour of 1.0 ppmv (around a height of 20 km) is estimated at about 1.1 ± 0.2 km month^{-1} for the period of focus of 26 September through 24 October 2003.

Next, the O_3 descent rate was examined as a function of longitude using ILAS-II data. Figure 6 shows the time–height sections of ozone mixing ratio for six longitude regions with a width of 60° made using only data in the deep vortex interior from ILAS-II observations. The downward movement of the contour in late September through late October is clear in all longitude regions. An interesting feature is that the O_3 descent rate is largely dependent on longitude, being faster in the sectors of 120°–180°E and 180°–240°E and slower in the sectors of 300°–360°E and 0°–60°E.

The O_3 descent rate is estimated by using the least squares method for the period of focus as a function of longitude. The estimation is also made for long-lived species N_2O and CH_4. It is considered that the N_2O and CH_4 descent rates represent the Brewer–Dobson circulation, assuming that irreversible mixing is absent. First, we examined these descent rates (km month^{-1}) by taking the geometric height as the vertical coordinate, for comparison with the vertical component of the residual circulation calculated using ECMWF data.

Results are shown in Fig. 7 for the height of ~20 km where all of the vertical gradients of the ozone, N_2O, and CH_4 mixing ratios are sufficiently large to estimate the descent rate. Contours of 1.0 ppmv for O_3, 30 ppbv for N_2O, and 0.6 ppmv for CH_4 were used. Note that "negative" descent rates mean "downward" movements in this figure. Marks outside the box show the zonal mean values (i.e., estimates using data at all longitudes). Error bars show 70% confidence limits of a t test. The vertical speed of the residual circulation is shown by a horizontal straight line. The magnitude of the vertical speed is in the range of the descent rate of long-lived species.

Longitudinal dependence in the descent rates is commonly observed for all species. The descent rates are largest around 210°E and smallest around 30°E. The O_3 descent rate at Syowa Station (1.1 km month^{-1}; an open circle) from ozonesonde observations almost accords with the ILAS-II observation around 30°E.

Another important feature is that the O_3 descent rates are larger than those for N_2O and CH_4 in most longitude regions except for sectors near 0°E, where the descent rates for all species almost accord. As a result, the zonal mean descent rate of ozone (2.6 km month^{-1}) is larger than those of N_2O and CH_4 (about 2.0 km month^{-1}).

b. *Dynamical interpretation in terms of slowly varying planetary waves*

To elucidate the mechanism causing longitudinal dependence in the descent rates, dynamical fields were examined using ECMWF operational data for the period of focus. Figures 8a and 8b show maps of the

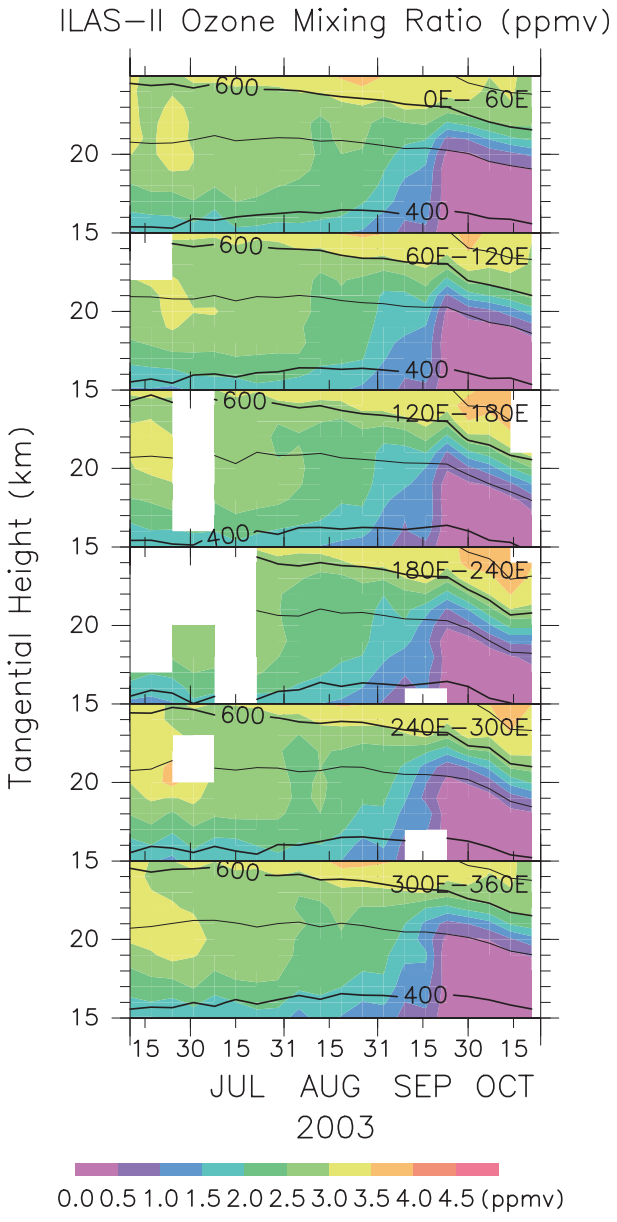

FIG. 6. Time–height sections of ozone mixing ratio (colors) and potential temperature (contours) inside the polar vortex for six different longitude regions based on ILAS-II observation data in 2003. Contour intervals are 100 K.

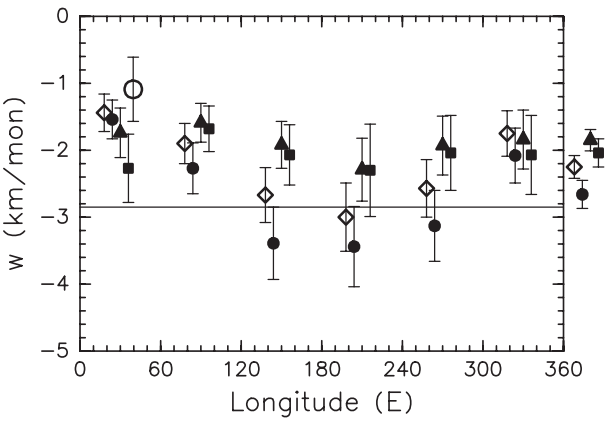

FIG. 7. Descent rates (km month^{-1}) in the polar vortex interior estimated using ILAS-II data as a function of longitude around a height of 20 km by taking the geometric height as the vertical coordinate in the period of focus from 26 Sep to 24 Oct 2003. Negative values show descent. Closed circles, closed triangles, and closed rectangles represent ozone (1.0 ppmv), N_2O (30 ppbv), and CH_4 (0.6 ppmv), respectively. Data points on the right (outside the box) show the zonal means. The horizontal line is the vertical component of diabatic circulation averaged for 70°–85°S. Open diamonds show the descent rates of isentropic surface of 500 K ($z \sim 20$ km). The marks except for N_2O are shifted slightly rightward or leftward for easier comparison. An open circle indicates the estimate from ozonesonde observations at Syowa Station. Error bars show 70% confidence limits.

time-mean geopotential height and the anomaly from its zonal mean at 50 hPa (around 20 km). A strong stratospheric polar vortex with its center shifting toward 30°E is observed in Fig. 8a. Corresponding to the vortex shift, a clear quasi-stationary planetary wave structure with a zonal wavenumber of 1 ($s = 1$) is seen in the anomaly field (Fig. 8b).

Figures 8c and 8d show time series of the amplitude of geopotential height fluctuations (mostly due to the $s = 1$ component) and unfiltered temperature as a function of longitude for the period of focus. The amplitude of geopotential height fluctuations increase gradually during the time period, although short-period variations are embedded (Fig. 8c). The temperature increases according to the seasonal variation of solar radiation (Fig. 8d). A temperature maximum is seen around 180°E, suggesting that the height of the isentropic surface is lower there. The temperature maximum (i.e., the phase of the $s = 1$ wave) drifts eastward slightly during the period of focus.

The amplitude increase and phase drift of the $s = 1$ planetary wave roughly account for the longitudinal variation of observed descent rates (Fig. 7). Figure 9 illustrates the mechanism. The upper curve shows a material surface at the beginning ($t = t_1$) of the period of focus as a function of longitude. The material surface is lower around 180°E because it is modulated by the $s = 1$ planetary wave. One month later ($t = t_2$), the material surface has descended as shown by the lower curve. The amplitude of undulation becomes larger and the phase shifts slightly eastward, corresponding to the observed time variation of the amplitude and phase of the planetary wave. The potential temperature of the material surface is higher at $t = t_2$ because of radiative heating in spring.

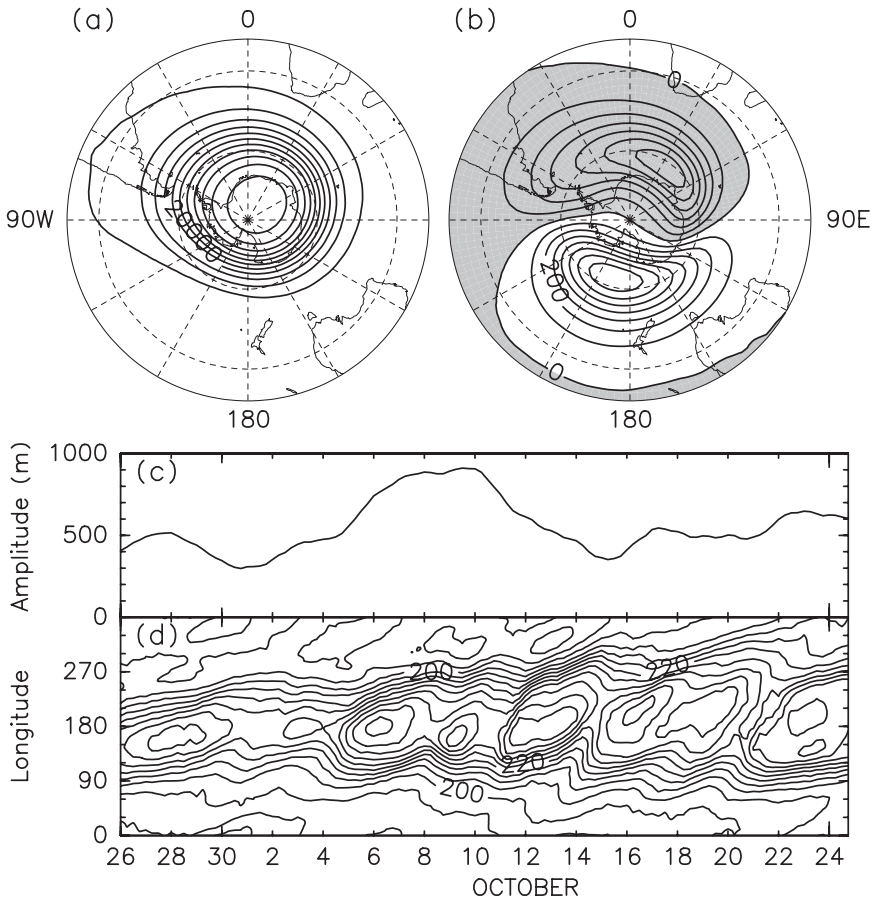

FIG. 8. Polar stereoprojection maps of (a) geopotential height and (b) anomaly from its zonal mean at 50 hPa averaged over 26 Sep–24 Oct 2003. (c) Time series of amplitude of the zonal wavenumber-1 geopotential height component. (d) A time–lon section of temperature at 70°S and 50 hPa. Contour intervals are 200 m in (a), 100 m in (b) and 5 K in (d). The regions with negative values are shaded in (b).

The descent rate of a particular mixing ratio contour of a long-lived species is considered to correspond to that of the material surface at each longitude as shown by thick arrows. The descent rate should be largest around the longitude of 210°E and smallest around 30°E, which is consistent with observations (Fig. 7). The descent rate of an isentropic surface (potential temperature surface) of 500 K calculated using ECMWF operational data is also shown in Fig. 7 by open rectangles as a function of longitude. The longitudinal variation of the descent rate is consistent with the illustration of Fig. 9. The mathematical formulation of the longitudinal dependence of the descent rate is given in the appendix.

It may be worth noting that the descent rate of the material surface differs from the planetary wave vertical wind component. The latter corresponds to the movement of air parcels on the material surface modified by the planetary wave, as shown by open circles with arrows in Fig. 9.

5. Longitudinal dependence of ozone increase in the isentropic vertical coordinate

a. Descent rates in the isentropic vertical coordinate

If the longitudinal dependence of observed descent rates for minor constituents is attributed only to the adiabatic modulation of the material surface by planetary waves, the descent rates estimated by taking the potential temperature as the vertical coordinate (K month^{-1}) should be constant (see the appendix). Descent rates around the isentropic surface of 500 K (~20 km) are shown in Fig. 10. It is clear that the descent rates for the isentropic coordinate still have longitudinal dependence. The error bars show 70% confidence limits. Note

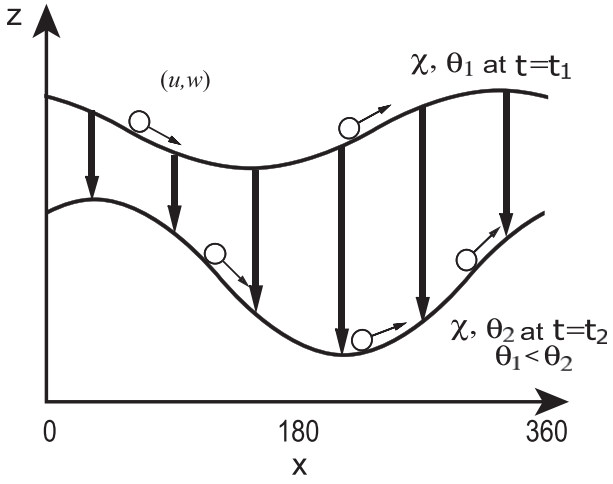

FIG. 9. A schematic illustration for the downward movement of a material surface (two thick curves for $t = t_1$ and $t = t_2$, respectively) modified by an $s = 1$ quasi-stationary planetary wave, which is amplified and phase-shifted eastward as observed. Thick downward arrows indicate the descent rates of the material surface of mixing ratio χ at respective lons in a month. Thin arrows with open circles illustrate the Lagrangian motion with zonal and vertical velocity components of u and w on the meandered material surface. Potential temperature of the material surface is shown as θ_1 for $t = t_1$ and θ_2 for $t = t_2$. Note that $\theta_2 > \theta_1$ because of the increase in solar heating in spring. See text for details.

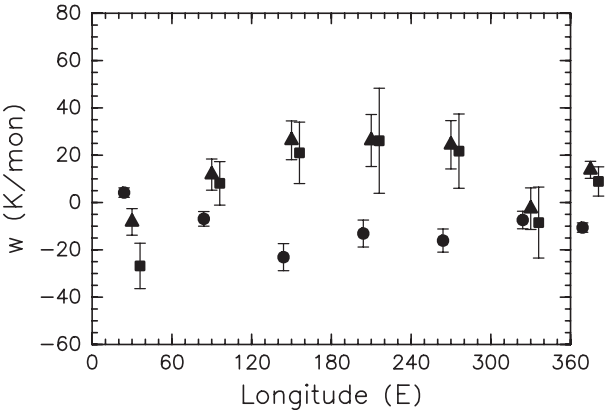

FIG. 10. As in Fig. 7, but for the descent rates (K month^{-1}) around an isentrope of 500 K by taking the potential temperature as the vertical coordinate. Negative (positive) values show descent (ascent).

that the estimation errors for N_2O and CH_4 are large compared with ozone because the vertical gradient of mixing ratio is not large for N_2O and CH_4 around 500 K (not shown in detail).

The O_3 descent rate is largely negative around 210°E and slightly positive (i.e., for the ascent relative to the isentrope) around 30°E. In other words, the increase in ozone is faster around 210°E even on the same isentropic surface. The N_2O and CH_4 descent rates are positive in most longitude regions except for those around 0°E. Because N_2O and CH_4 are chemically inactive in this height region, the longitudinal dependence of their descent rates indicates that there exist dynamical processes causing inhomogeneity on isentropic surfaces (such as lateral mixing).

b. Possibility of lateral mixing

Plumb et al. (2000) suggest the possibility of lateral mixing of outside air into the polar vortex before the vortex breakup using a conceptual model and three-dimensional chemical transport models. To see the origin of the air parcels reaching each observed-longitude region, backward trajectories on the isentropic surface of 500 K over 5 days were examined, for which the adiabatic assumption is considered to be almost valid in the lower stratosphere. The National Institute of Polar Research (NIPR) trajectory model (Tomikawa and Sato 2005) was used for these calculations. The initial locations for the backward trajectory calculation were the ILAS-II observational points in the deep vortex interior.

The results are shown in Figs. 11a,b for the longitude regions of 0°–60°E and 180°–240°E, respectively. Figure 11c shows a map of total column ozone averaged over 1–15 October 2003 that is made from Total Ozone Mapping Spectrometer (TOMS)/Earth Probe observation data. The trajectories in the two regions are very different. The backward trajectories starting between 180° and 240°E passed lower latitude regions close to the edge of the polar vortex, suggesting the possibility of strong lateral mixing with the ozone-rich air in lower latitudes. On the other hand, the trajectories for 0°–60°E were mostly situated in the polar vortex interior, suggesting that lateral mixing with ozone-rich air hardly occurred.

Tracer–tracer correlation analysis is useful to detect the existence of irreversible mixing (Plumb and Ko 1992; Shepherd 2007). The ozone destruction processes in 2003 were examined in detail using this method by Tilmes et al. (2006), for example. The occurrence of lateral mixing during the period of focus may be confirmed by temporal variation of scatter diagrams for mixing ratios of two minor constituents. Figure 12 shows scatter diagrams of O_3 versus N_2O in three time periods: 26 September to 5 October (period I), 6–15 October (period II), and 16–24 October 2003 (period III). The data points are plotted by different colors for different isentropic levels. In period I, the distribution of data points at all isentropic levels is compact (i.e., forming a curve). In periods II and III, the distribution of data points becomes dispersed. Data points around 210°E, which have backward trajectories reaching lower latitudes,

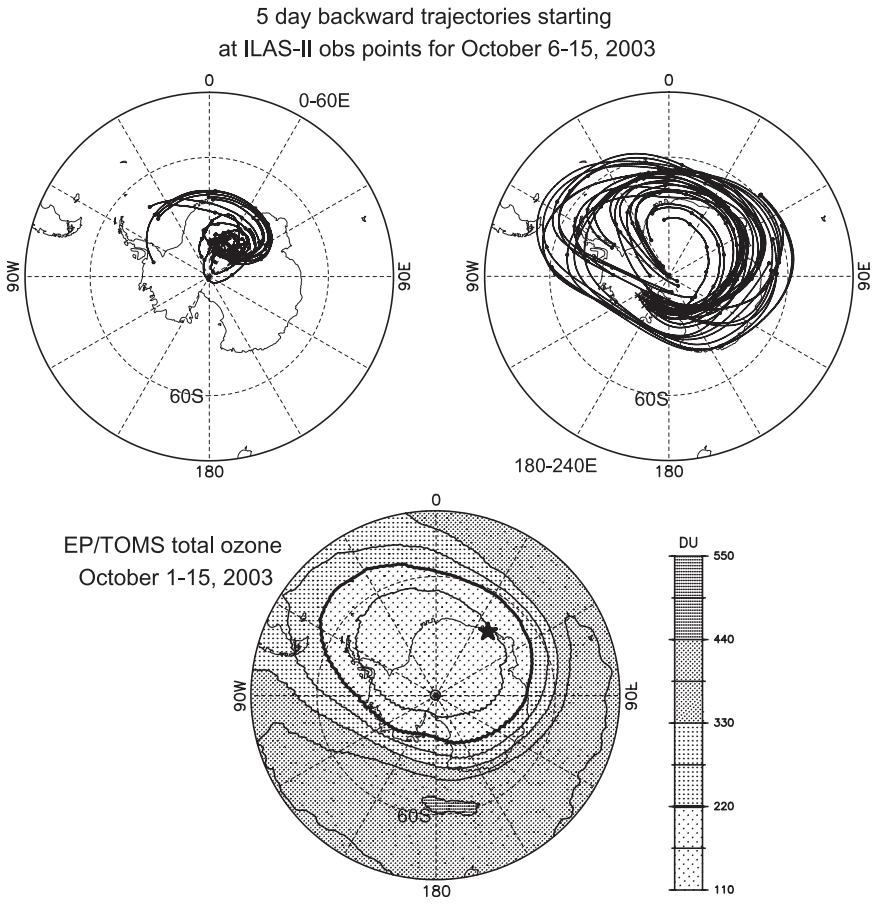

FIG. 11. Backward trajectories (solid curves) over 5 days starting at ILAS-II observational points (cross marks) in the sectors (a) 0°–60°E and (b) 180°–240°E over the period 6–15 Oct 2003 on the isentropic surface of 500 K. Dots are plotted for each day. (c) A map of total ozone averaged over 1–15 Oct 2003. A star mark shows the location of Syowa Station.

are distributed far from the original curve (not shown). This result also indicates that strong mixing occurred for the air parcels observed around 210°E during the period of focus.

It is worth noting here that because both N_2O and CH_4 (O_3) mixing ratios have a negative (positive) gradient with height and large values outside the polar vortex, the strong positive (negative) descent rates around 210°E are consistent with the inference of strong lateral mixing.

c. *Contribution of lateral mixing to the ozone recovery*

The contribution of the lateral mixing to the increase in ozone can be roughly estimated using the descent rates in both the geometric and isentropic vertical coordinates (Figs. 7 and 10). The zonal mean descent rate of the isentropic layer in the geometric coordinate is -2.25 km month^{-1} (Fig. 7). The descent rates in the isentropic coordinate shown in Fig. 10 are relative to this mean descent rate of the isentropic layer. The descent rate in the isentropic coordinate can be translated to that in the geometric coordinate using the fact that a potential temperature difference of 100 K corresponds to an altitude difference of 2.5 km around the height of 20 km (e.g., Fig. 6). The region with air that is least subject to lateral mixing should have the smallest O_3 descent rate in Fig. 10 because the ozone mixing ratio has a positive gradient with height and large values outside the polar vortex. Thus, it is considered that the downward transport by the Brewer–Dobson circulation is reflected in the O_3 descent rate around 30°E, namely $+4.2$ K month^{-1}. This value is equivalent to the descent rate of 0.105 km month^{-1}. The true descent rate due to the Brewer–Dobson circulation is therefore estimated at -2.145 ($= -2.25 + 0.105$) km month^{-1}.

On the other hand, the zonal mean O_3 descent rate of -10.6 K month^{-1} (equivalent to -0.265 km month^{-1};

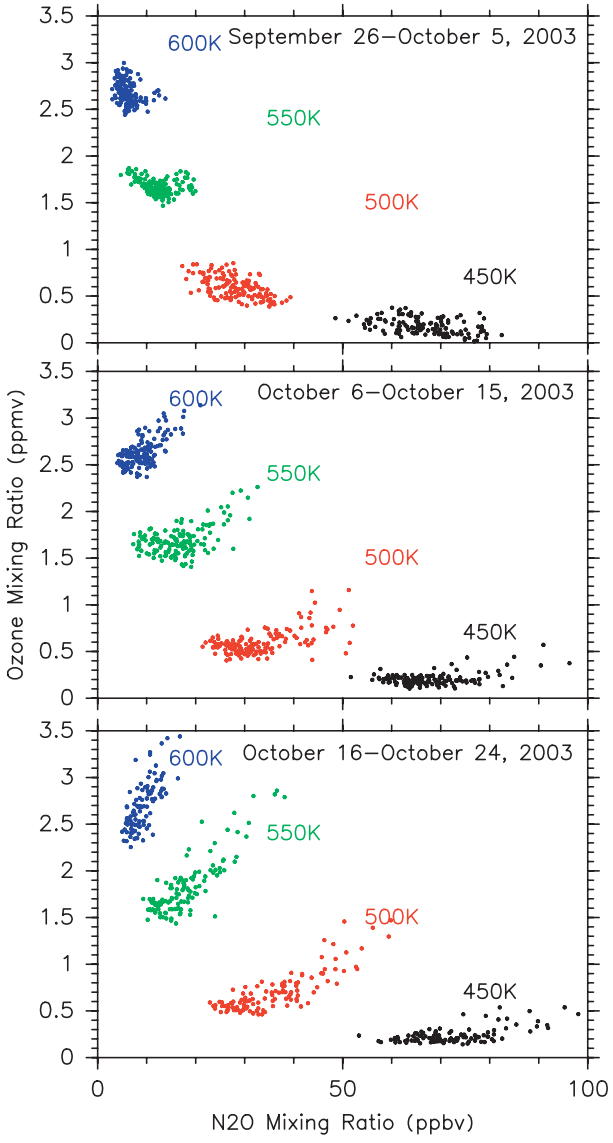

FIG. 12. Scatter diagrams of O_3 and N_2O mixing ratios for 10-day periods. Different colors show results at isentropic levels of 600, 550, 500, and 450 K.

Fig. 10) is an "apparent" one because it includes the effect of lateral mixing. Thus, the contribution of lateral mixing to the apparent descent rate is -0.370 ($= -0.265 - 0.105$) km month^{-1}. This is about 17% of the true descent rate of -2.145 km month^{-1} by the Brewer–Dobson circulation, with an ambiguity of $\pm 4\%$ (corresponding to the error bars). Assuming that the vertical gradient of ozone mixing ratio is locally constant, this percentage is considered to be the contribution of lateral mixing to the increase in ozone around the height of 20 km.

The descent rates for all species should accord in the region where the lateral mixing is not significant. Such accordance is not clear around 30°E in Fig. 10. However, we used the O_3 descent rate around 30°E to estimate true descent rate due to the Brewer–Dobson circulation for the following reasons. First, the O_3 descent rate is most accurate of the three estimates, as shown by the error bars in Fig. 10. Larger error bars in the estimates for N_2O and CH_4 are due to the smaller vertical gradients of their mixing ratios. Second, the backward trajectories of air parcels around 30°E do not cross the polar vortex boundary region, unlike those in the other longitude regions, including a 330°E sector where the three descent rates match within the confidence limits (not shown in detail). Third, the "positive" value of the O_3 descent rate around 30°E is consistent with the temperature increase on a seasonal scale (see Fig. 9).

6. Summary and concluding remarks

The horizontal structure of processes causing increases in ozone in the Antarctic polar vortex was examined using data from an ozonesonde observation campaign at Syowa Station (69.0°S, 39.6°E) and from the Improved Limb Atmospheric Spectrometer-II (ILAS-II) onboard the *Advanced Earth Observing Satellite II* (*ADEOS-II*) measured in 2003, when one of the largest ozone holes recorded appeared. The analysis was focused on the period from 26 September through 24 October, when a strong polar vortex was situated in the lower stratosphere.

A clear downward movement was observed for an ozone mixing ratio contour around the altitude of 20 km in the polar vortex interior during this period. The descent rate was estimated for six adjacent longitudinal sectors with a longitudinal width of 60°, utilizing the ILAS-II data (which is distributed uniformly in the zonal direction). It was clear that the O_3 descent rate for the geometric vertical coordinate had significant longitudinal dependence. A similar feature was observed for long-lived species N_2O and CH_4. Results of the analysis of dynamical fields using ECMWF operational data showed that the longitudinal dependence was roughly explained by longitudinally dependent vertical movements of the isentropes modified by a zonal wavenumber-1 quasi-stationary planetary wave with amplitude and phases varying on a seasonal time scale.

The longitudinal dependence was also present when the O_3 descent rate was estimated for the isentropic vertical coordinate, meaning that the increase in ozone was largely dependent on longitude over isentropic surfaces even before the polar vortex breakup. Longitudinal dependence was also present for the N_2O and CH_4 descent rates in the isentropic vertical coordinate.

A backward trajectory analysis was made for air parcels reaching each longitudinal sector. The results indicated that the trajectories of air parcels were very

different because of the dominance of a quasi-stationary planetary wave. The trajectories of most air parcels with large ozone mixing ratios in the longitudinal sector around 210°E passed near the polar vortex boundary region, whereas most trajectories for the air parcels with small mixing ratios in the sector around 30°E were situated in the deep vortex interior. This fact suggests that lateral transport/mixing is important for ozone increase even in the period when a strong polar vortex is present in the stratosphere. Tracer–tracer correlation analysis of O_3 and N_2O also indicated the presence of irreversible mixing during this period.

A rough estimate of the contribution of lateral mixing to the increase in ozone was 17% ± 4% that due to the Brewer–Dobson circulation. The results of this study also imply that Lagrangian downward motions are not correctly estimated using inactive minor constituents without accounting for lateral mixing even when the polar vortex is stable.

As of yet, the transport of minor constituents in the lower stratosphere has been mainly examined in meridional cross sections, and the processes causing three-dimensional features as shown in the present study have not been investigated in detail. Gravity waves and medium-scale trapped waves that are dominant around the polar vortex (Pfenninger et al. 1999; Yoshiki and Sato 2000; Yoshiki et al. 2004; Sato and Yoshiki 2008; Tomikawa and Sato 2003) may be important for three-dimensional transport processes. The use of high-resolution global model simulation (e.g., Sato et al. 1999; Watanabe et al. 2008; Tomikawa et al. 2008) may provide an interesting avenue for investigating this issue in detail.

Acknowledgments. The intensive ozonesonde observation was made as part of research by the 44th Japanese Antarctic Research Expedition (JARE44), in which the first author (KS) participated. Thanks are due to Masaki Tsutsumi and Naohiko Hirasawa of National Institute of Polar Research and Isao Murata of Tohoku University for their domestic support of the experiments, and also to Michiyoshi Namiki, Yukihiko Matsuzaka, and Takamasa Yamagami for their help for high-altitude balloon observations. Some of the ECC ozonesondes used in this study were provided by the QUOBI project. The ILAS-II project was funded by the Ministry of the Environment of Japan (MOE). We are grateful to Hideharu Akiyoshi and Makoto Koike for their valuable discussion. We also thank for two anonymous reviewers for their careful reading and constructive comments. The GFD-DENNOU library was used for drawing figures. Operational analysis data used in this study were provided by ECMWF. TOMS/EP data were provided by NASA. Ozone hole area data were provided by JMA. This study was supported by Grant-in-Aid for Scientific Research (C) 17540417 and (A) 19204047 of the Ministry of Education, Culture, Sports and Technology, Japan and by a Global Environment Research Fund (A-04-10) of the MOE.

APPENDIX

Mathematical Formulation of the Descent Rate as a Function of Longitude

In this section, we formulate the mechanism of longitudinally dependent descent rates in the presence of a planetary wave. The descent rate for the geometric vertical coordinate $(\partial z/\partial t)_\chi$ (Fig. 7) and that for the isentropic vertical coordinate $(\partial\theta/\partial t)_\chi$ (Fig. 10) are related through the following identity:

$$\left(\frac{\partial\theta}{\partial t}\right)_\chi = \left(\frac{\partial\theta}{\partial t}\right)_z + \left(\frac{\partial\theta}{\partial z}\right)_t \left(\frac{\partial\theta}{\partial t}\right)_\chi, \tag{A1}$$

where θ is the potential temperature, t is time, z is geometric height, and χ is the mixing ratio of a long-lived tracer. Here we ignored lateral mixing for simplicity. Because θ is constant over the material surface,

$$(\nabla\theta)_\chi = 0. \tag{A2}$$

Thus,

$$\left(\frac{\partial\theta}{\partial t}\right)_\chi = \left(\frac{D\theta}{Dt} - \mathrm{v}\cdot\nabla\theta\right)_\chi = Q. \tag{A3}$$

Because air parcels rotate around the pole many times, the diabatic heating $Q(\equiv D\theta/Dt)$ averaged over a month as examined in the present study can be considered to be constant. Thus, $(\partial\theta/\partial t)_\chi$ does not depend on longitude. Next, we assume that the potential temperature has a shape of $\theta = \Theta(t)e^{ik(x-ct)}$ as observed, where $\Theta(t)$ is the time-dependent amplitude, x is the zonal coordinate, k is zonal wavenumber, and c is zonal phase speed. Then

$$\left(\frac{\partial\theta}{\partial t}\right)_z = \left[e^{ik(x-ct)}\frac{\partial\Theta}{\partial t} + \Theta\frac{\partial e^{ik(x-ct)}}{\partial t}\right]_z \tag{A4}$$

$$= \left[e^{ik(x-ct)}\frac{\partial\Theta}{\partial t} + c\frac{\partial\theta}{\partial x}\right]_z \tag{A5}$$

$$= \left(\frac{\theta}{\Theta}\frac{\partial\Theta}{\partial t} + c\frac{\partial\theta}{\partial x}\right)_z. \tag{A6}$$

Moreover, for simplicity, we assume that the vertical gradient of potential temperature is constant (Λ):

$$\left(\frac{\partial\theta}{\partial z}\right)_t = \Lambda. \tag{A7}$$

Using (A3), (A6), and (A7), (A1) becomes

$$Q = \left(\frac{\theta}{\Theta}\frac{\partial\Theta}{\partial t} + c\frac{\partial\theta}{\partial x}\right)_z + \Lambda\left(\frac{\partial z}{\partial t}\right)_\chi. \quad \text{(A8)}$$

Thus,

$$\left(\frac{\partial z}{\partial t}\right)_\chi = \frac{1}{\Lambda}\left[Q - \left(\frac{\theta}{\Theta}\frac{\partial\Theta}{\partial t} + c\frac{\partial\theta}{\partial x}\right)_z\right]. \quad \text{(A9)}$$

This equation shows how the descent rates at respective longitudes are related to the temporally varying amplitude, zonal phase speed, and zonal phase structure of the planetary wave.

REFERENCES

Abrams, M. C., and Coauthors, 1996: ATMOS/ATLAS-3 observations of long-lived tracers and descent in the Antarctic vortex in November 1994. *Geophys. Res. Lett.,* **23,** 2341–2344.

Andrews, D. G., J. R. Holton, and C. B. Leovy, 1987: *Middle Atmosphere Dynamics*. Academic Press, 504 pp.

Chubachi, S., 1984: Preliminary result of ozone observations at Syowa station from February 1982 to January 1983. *Mem. Natl. Inst. Polar Res.,* **34,** 13–19.

Ejiri, M. K., and Coauthors, 2006: Validation of the Improved Limb Atmospheric Spectrometer-II (ILAS-II) version 1.4 nitrous oxide and methane profiles. *J. Geophys. Res.,* **111,** D22S90, doi:10.1029/2005JD006449.

Farman, J. C., B. G. Gardiner, and J. D. Shanklin, 1985: Large losses of total ozone in Antarctica reveal seasonal ClO_x/NO_x interaction. *Nature,* **315,** 207–210.

Holton, J. R., P. H. Haynes, M. E. McIntyre, A. R. Douglass, R. B. Rood, and L. Pfister, 1995: Stratosphere–troposphere exchange. *Rev. Geophys.,* **33,** 403–439.

Jacob, D. J., 1999: *Introduction to Atmospheric Chemistry*. Princeton University Press, 264 pp.

Kawamoto, N., and M. Shiotani, 2000: Interannual variability of the vertical descent rate in the Antarctic polar vortex. *J. Geophys. Res.,* **105,** 11 935–11 946.

——, H. Kanzawa, and M. Shiotani, 2004: Time variations of descent in the Antarctic vortex during the early winter of 1997. *J. Geophys. Res.,* **109,** D18309, doi:10.1029/2004JD004650.

Manney, G. L., R. W. Zurek, L. Froidevaux, J. W. Waters, A. O'Neill, and R. Swinbank, 1995: Lagrangian transport calculations using *UARS* data. Part II: Ozone. *J. Atmos. Sci.,* **52,** 3069–3081.

McElroy, M. B., R. J. Salawitch, S. C. Wofsy, and J. A. Logan, 1986: Reductions of Antarctic ozone due to synergistic interactions of chlorine and bromine. *Nature,* **321,** 759–762.

Molina, L. T., and M. J. Molina, 1987: Production of Cl_2O_2 from the self-reaction of the ClO radical. *J. Phys. Chem.,* **91,** 433–436.

Murata, I., K. Sato, T. Yamagami, S. Okano, M. Tsutsumi, K. Noguchi, and H. Fukunishi, 2004: Development of a balloon-borne optical ozone sensor with GPS receiver. *Proc. 20th Quadrennial Ozone Symp.,* Kos, Greece, WMO, 587–588.

Nakajima, H., T. Sugita, T. Yokota, and Y. Sasano, 2005: Atmospheric environment monitoring by the ILAS-II onboard the ADEOS-II satellite. *Remote Sensing of Clouds and the Atmosphere IX*, A. Comeron et al., Eds., International Society for Optical Engineering (SPIE Proceedings, Vol. 5571), 293–300.

——, and Coauthors, 2006: Characteristics and performance of the Improved Limb Atmospheric Spectrometer-II (ILAS-II) on board the ADEOS-II satellite. *J. Geophys. Res.,* **111,** D11S01, doi:10.1029/2005JD006334.

Nash, E. R., P. A. Newman, J. E. Rosenfield, and M. R. Schoeberl, 1996: An objective determination of the polar vortex using Ertel's potential vorticity. *J. Geophys. Res.,* **101,** 9471–9478.

Okano, S., M. Okabayashi, and H. Gernandt, 1996: Observations of ozone profiles in the upper stratosphere using a UV sensor on board a lightweight high-altitude balloon. *Mem. Natl. Inst. Polar Res.,* **51,** 225–231.

Pfenninger, M., A. Z. Liu, G. C. Papem, and C. S. Gardner, 1999: Gravity wave characteristics in the lower atmosphere at the South Pole. *J. Geophys. Res.,* **104,** 5963–5984.

Plumb, R. A., and M. K. W. Ko, 1992: Interrelationships between mixing ratios of long-lived stratospheric constituents. *J. Geophys. Res.,* **97,** 10 145–10 156.

——, D. W. Waugh, and M. P. Chipperfield, 2000: The effects of mixing on tracer relationships in the polar vortices. *J. Geophys. Res.,* **105,** 10 047–10 062.

Pope, F. D., J. C. Hansen, K. D. Bayes, R. R. Friedl, and S. P. Sander, 2007: Ultraviolet absorption spectrum of chlorine peroxide, ClOOCl. *J. Phys. Chem.,* **111A,** 4322–4332, doi:10.1021/jp067660w.

Rex, M., R. J. Salawitch, P. von der Gathen, N. R. P. Harris, M. Chipperfield, and B. Naujokat, 2004: Arctic ozone loss and climate change. *Geophys. Res. Lett.,* **31,** L04116, doi:10.1029/2003GL018844.

Rosenfield, J. E., P. A. Newman, and M. R. Schoeberl, 1994: Computations of diabatic descent in the stratospheric polar vortex. *J. Geophys. Res.,* **99,** 16 677–16 689.

Sato, K., and M. Yoshiki, 2008: Gravity wave generation around the polar vortex in the stratosphere revealed by 3-hourly radiosonde observations at Syowa Station. *J. Atmos. Sci.,* **65,** 3719–3735.

——, T. Kumakura, and M. Takahashi, 1999: Gravity waves appearing in a high-resolution GCM simulation. *J. Atmos. Sci.,* **56,** 1005–1018.

Schoeberl, M. R., M. Z. Lu, and J. E. Rosenfield, 1995: An analysis of the Antarctic Halogen Occultation Experiment trace gas observations. *J. Geophys. Res.,* **100,** 5159–5172.

Shepherd, T. G., 2007: Transport in the middle atmosphere. *J. Meteor. Soc. Japan,* **85B,** 165–191.

Solomon, S., 1999: Stratospheric ozone depletion: A review of concepts and history. *Rev. Geophys.,* **37,** 275–316.

Sugita, T., and Coauthors, 2006: Ozone profiles in the high-latitude stratosphere and lower mesosphere measured by the Improved Limb Atmospheric Spectrometer (ILAS)-II: Comparison with other satellite sensors and ozonesondes. *J. Geophys. Res.,* **111,** D11S02, doi:10.1029/2005JD006439.

Tilmes, S., R. Müller, J.-U. Grooss, R. Spang, T. Sugita, H. Nakajima, and Y. Sasano, 2006: Chemical ozone loss and related processes in the Antarctic winter 2003 based on Improved Limb Atmospheric Spectrometer (ILAS)-II observations. *J. Geophys. Res.,* **111,** D11S12, doi:10.1029/2005JD006260.

Tomikawa, Y., and K. Sato, 2003: Trapped waves in the edge region of stratospheric polar vortices. *J. Geophys. Res.,* **108,** 4047, doi:10.1029/2002JD002579.

——, and ——, 2005: Design of the NIPR trajectory model. *Polar Meteor. Glaciol.,* **19,** 120–137.

——, ——, S. Watanabe, Y. Kawatani, K. Miyazaki, and M. Takahashi, 2008: Wintertime temperature maximum at the subtropical

stratopause in a T213L256 GCM. *J. Geophys. Res.,* **113,** D17117, doi:10.1029/2008JD009786.

Tung, K. K., M. K. W. Ko, J. M. Rodriguez, and N. D. Sze, 1986: Are Antarctic ozone variations a manifestation of dynamics or chemistry? *Nature,* **322,** 811–814.

von der Gathen, P., and Coauthors, 1995: Observational evidence for chemical ozone depletion over the Arctic in winter 1991–92. *Nature,* **375,** 131–134.

von Hobe, M., 2007: Revisiting ozone depletion. *Science,* **318,** 1878–1879, doi:10.1126/science.1151597.

Watanabe, S., Y. Kawatani, Y. Tomikawa, K. Miyazaki, M. Takahashi, and K. Sato, 2008: General aspects of a T213L256 middle atmosphere general circulation model. *J. Geophys. Res.,* **113,** D12110, doi:10.1029/2008JD010026.

Yamagami, T., Y. Saito, Y. Matsuzaka, M. Namiki, M. Toriumi, T. Yokota, H. Hirosawa, and K. Matsushima, 2004: Development of the highest altitude balloon. *Adv. Space Res.,* **33,** 1653–1659.

Yoshiki, M., and K. Sato, 2000: A statistical study of gravity waves in the polar regions based on operational radiosonde data. *J. Geophys. Res.,* **105** (D14), 17 995–18 011.

——, N. Kizu, and K. Sato, 2004: Energy enhancements of gravity waves in the Antarctic lower stratosphere associated with variations in the polar vortex and tropospheric disturbances. *J. Geophys. Res.,* **109,** D23104, doi:10.1029/2004JD004870.